Free Radical Biology and Medicine 101 (2016) 85–92

Contents lists available at ScienceDirect

Free Radical Biology and Medicine

journal homepage: www.elsevier.com/locate/freeradbiomed

Imaging of radicals following injury or acute stress in peripheral nerves with activatable fluorescent probes

Haiying Zhou[a], Ying Yan[b], Xueping Ee[b], Daniel A. Hunter[b], Walter J. Akers[a,*,1], Matthew D. Wood[b,*,1], Mikhail Y. Berezin[a,*,1]

[a] Division of Radiation Sciences, Department of Radiology, Washington University School of Medicine, 4515 McKinley Avenue, St. Louis, MO 63110, USA
[b] Division of Plastic and Reconstructive Surgery, Department of Surgery, Washington University School of Medicine, 660 South Euclid Avenue, St. Louis, MO 63110, USA

ARTICLE INFO

Keywords:
ROS
Fluorescence
IFOS
Imaging
Peripheral nerve
Stress
Axons
Nerve histomorphometry

ABSTRACT

Peripheral nerve injury evokes a complex cascade of chemical reactions including generation of molecular radicals. Conversely, the reactions within nerve induced by stress are difficult to directly detect or measure to establish causality. Monitoring these reactions in vivo would enable deeper understanding of the nature of the injury and healing processes. Here, we utilized near-infrared fluorescence molecular probes delivered via intraneural injection technique to enable live, in vivo imaging of tissue response associated with nerve injury and stress. These initially quenched fluorescent probes featured specific sensitivity to hydroxyl radicals and become fluorescent upon encountering reactive oxygen species (ROS). Intraneurally delivered probes demonstrated rapid activation in injured rat sciatic nerve but minimal activation in normal, uninjured nerve. In addition, these probes reported activation within sciatic nerves of living rats after a stress caused by a pinprick stimulus to the abdomen. This imaging approach was more sensitive to detecting changes within nerves due to the induced stress than other techniques to evaluate cellular and molecular changes. Specifically, neither histological analysis of the sciatic nerves, nor the expression of pain and stress associated genes in dorsal root ganglia could provide statistically significant differences between the control and stressed groups. Overall, the results demonstrate a novel imaging approach to measure ROS in addition to the impact of ROS within nerve in live animals.

1. Introduction

Acute physical and psychological stress activates the sympathetic nervous system (i.e. “flight or fight” response) to facilitate rapid preparation of an animal's body for efforts to minimize injury and pain. Characteristic elements of this response to stress include a pressor reflex, increased heart rate and blood pressure, alongside elevated neuro-excitability in muscle tissues [1]. Yet, while elements of this response provide useful functions, select mediators of the stress can have deleterious consequences to the nervous system through promotion of cellular damage and inflammation.

Potent mediators of the stress response are molecular radicals, including reactive oxygen species (ROS), which signal a diverse range of biological processes and the type of stress [2,3]. Whereas radical signaling plays an essential role in cellular functions, endogenous mechanisms that normally repair oxidative damage can be overwhelmed by excess accumulation of ROS leading to oxidative damage of lipids, proteins, and nucleic acids. Damage to these essential cellular components is associated with a range of conditions and diseases including cancer, aging, and inflammation [4]. Indeed, even psychological stress has been shown to cause oxidative damage to nuclear DNA [5–7]. Beyond direct damage to cellular components, ROS is a potent immune and inflammatory modulator. Radical damage from ROS is associated with multiple diseases within the neurological spectrum: Alzheimer's disease [8], multiple sclerosis [9], amyotrophic lateral sclerosis [10], and post-traumatic stress disorder (PTSD) [11].

Abbreviations: CNS, central nervous system; PNS, peripheral nervous system; NIR, near-infrared; ROS, reactive oxygen species; HITC, 1,1′,3,3,3′,3′-hexamethylindotricarbocyanine; HITC-H, reduced, activatable form of HITC; DMSO, dimethyl sulfoxide; TMS, tetramethylsilane; TFA, trifluoroacetic acid; IP, intraperitoneal; DRG, dorsal root ganglia; NGF, nerve growth factor; LC/MS-ESI, liquid chromatography mass spectrometer electron spray ionization; ROI, region of interest; iFOS, integrated Fluorescence Overpotential Spectroscopy; CRH, corticotropin-releasing hormone

* Corresponding authors.
E-mail addresses: akersw@wustl.edu (W.J. Akers), woodm@wudosis.wustl.edu (M.D. Wood), berezinm@wustl.edu (M.Y. Berezin).
[1] These authors contributed equally to the manuscript and are co-senior authors.

http://dx.doi.org/10.1016/j.freeradbiomed.2016.09.028
Received 15 July 2016; Received in revised form 27 September 2016; Accepted 27 September 2016
Available online 28 September 2016

Oxidative stress is also implicated as an initiating factor in numerous peripheral neuropathies including chemotherapy-induced peripheral neuropathy [12] and diabetic neuropathy [13]. Yet, the role of oxidative stress associated with the onset of these peripheral neurological conditions, including stress, has been challenging to fully establish as causal as its measurement requires sensitive assays that have not been amenable to in vivo use.

The full implications of radical accumulation in peripheral nerves are not completely understood as methods to monitor ROS dynamically and locally are underdeveloped. Blood flow to the peripheral nervous system is highly regulated through semi-permeable blood-nerve barriers, which decrease the sensitivity of serum marker measurements [14,15]. In addition, current preclinical techniques are unable to provide direct assessment of toxic radicals within peripheral nerves. Damage to lipids, proteins, and nucleic acids can be readily measured in ex vivo tissues [16,17] and through numerous sensitive assays relying on blood or serum [18,19], but tissue-specific and serial monitoring of radical expression in real time is not readily available due to the short half-life of ROS [2]. This inability to monitor ROS dynamically within a tissue of interest hinders evaluations of treatments intended to minimize the damage and demonstrate causal evidence of disease progression or submission. Traditional visible activatable imaging probes (i.e. dihydrodichlorofluorescein, dihydrorhodamine) are unsuitable for in vivo applications due to interference from tissue autofluorescence as well as low photon penetration. Recently near-infrared (NIR) activatable probes from the class of hydrocyanines suitable for ROS monitoring in live animals were proposed [20] and utilized for in vivo imaging of ischemia [21], acute lung injury [22], uncontrolled gut inflammation [23], and inflammation associated with implants [24].

In this work, we have developed an imaging approach for detecting ROS in the nerve tissue of live animal models using NIR activatable probes to evaluate an acute stress response. A focused NIR probe library was generated to provide a rationale selection of imaging agents. Considering chemical and biological properties of nerve tissues, we selected a probe that would allow for the semi-quantitative measurement of ROS generation within nerve. The presented imaging approach was sensitive enough to measure ROS activation in the nerve tissue following a relatively mild, acute stressful event. The observed fluorescent signals were detected despite minimal changes to sensory neurons and their axons within the peripheral nervous system (PNS), representing a potentially powerful tool for uncovering biological mechanisms underlying the onset of pathologies.

2. Experimental

2.1. Materials and methods

2.1.1. General information

Common solvents and reagents for synthesis were purchased from Sigma-Aldrich, Alfa Aesar, or TCI America and used without further purification. Dyes 1,1′,3,3,3′,3′-hexamethylindotricarbocyanine (HITC) was purchased from Exciton, IRDye800CW from LI-COR Biosciences, ADS740WS was obtained from American Dye Source, LS851 was prepared in the lab according to a standard cyanine synthesis procedure [25]. Reduced hydrocyanines HITC-H, IRdye800CW-H, ADS740WS−H, and LS851-H (Fig. 1) were prepared according to a previously published procedure [20]. NMR spectra were recorded at room temperature on a Varian 400 MHz system in dimethyl sulfoxide (DMSO) with tetramethylsilane (TMS) as an internal standard (unless noted otherwise). Milli-Q water (Millipore) was used throughout this work. The compounds were analyzed using LC/MS-ESI analysis in the positive mode conducted on a Shimadzu 2010 A LC/MS system equipped with a UV/Vis detector at different wavelengths using a reversed-phase C-18 Vydac column (model 218TP, 4.6×50 mm) at a flow rate of 0.7 mL/min with a gradient of 10–95% acetonitrile in water (both solvent contained 0.1% trifluoroacetic acid (TFA)). UV/Vis spectra of samples were recorded on a DU 640 spectrophotometer (Beckman Coulter). Steady state fluorescence spectra were recorded on a Fluorolog-3 spectrofluorometer (Horiba Jobin Yvon).

2.1.2. Hydrocyanines synthesis, general procedure

To produce activatable non-fluorescent hydrocyanine dyes for ROS detection, each dye (0.028 mmol) was dissolved in methanol (7 mL) and put on ice. Sodium borohydrate ($NaBH_4$) (0.113 mmol) was added to methanol (0.5 mL) on ice and the $NaBH_4$ solution was added dropwise to the dye-methanol solution with stirring. The reaction was monitored by the disappearance of the maximum absorption band using UV/Vis spectroscopy. The reaction was then warmed to room temperature (r.t.) with stirring over 20 min. The solvent was removed under vacuum to yield the final product (Scheme 1).

2.1.3. Optical properties

For calculating the concentration from the absorption spectra, molar absorptivities of hydrocyanine probes were measured in a quartz cuvette with a known concentration of the dye in the original, oxidized form according to the formula:

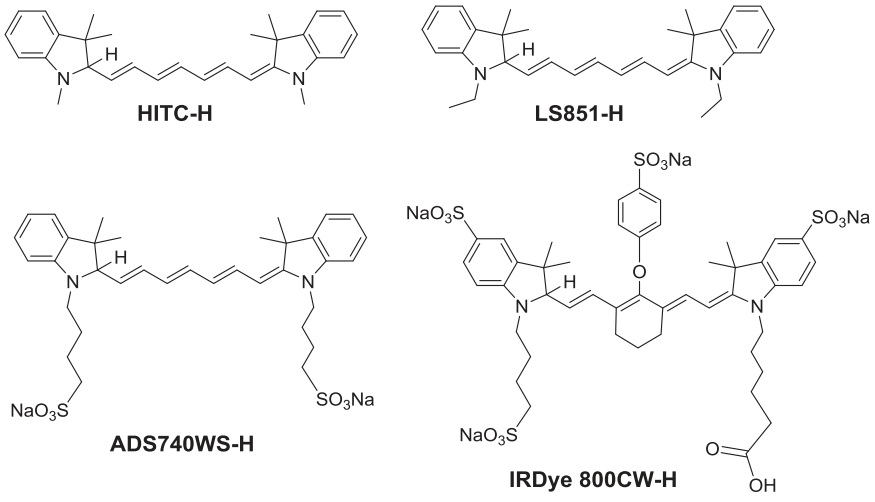

Fig. 1. Structures of the synthesized NIR activatable probes. HITC-H and LS851-H are hydrophobic molecules; ADS740WS-H and IRDye 800CW-H are hydrophilic due to the presence of sulfonate groups.

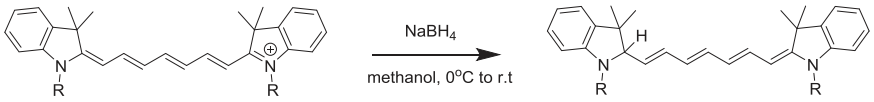

Scheme 1. Synthesis of NIR activatable probes hydrocyanines sensitive to ROS.

$$\epsilon_{red}=\epsilon_{ox}\frac{A_{395}^{after}-A_{395}^{before}}{A_{768}^{after}-A_{768}^{before}}$$

where ε_{red} is the molar absorptivity of the ROS probe in ethanol, M^{-1} cm^{-1}, ε_{ox} is the molar absorptivity of the dye, that was measured using standard weight method and power plot, A_{768} – is the absorption at 768 nm before and after reduction, A_{395} - is the absorption at 395 nm before and after reduction. The molar absorptivity for HITC-H is 68,000 M^{-1} cm^{-1} and 159,600 M^{-1} cm^{-1} for HITC.

2.1.4. NIR integrated Fluorescence Overpotential Spectroscopy (iFOS)

The sensitivity of the dye to ROS was performed spectroelectrochemically using an in-house built iFOS technique [26] modified for NIR studies with a light-emitting diode (LED) 725 nm (Thorlabs) as the source of excitation. The method combines spectroscopic measurements with an electrochemical method of oxidation to measure the threshold oxidation potential of leuco-dyes. The three-electrode electrochemical cell was comprised of a polystyrene cuvette with a glassy carbon working electrode (d=2 mm, CH Instruments), Pt-wire counter electrode, and Ag/AgCl reference electrode filled with a filling solution comprised of 3 M NaCl and saturated AgCl (Princeton Applied Research). The electrodes were inserted in a custom designed and made on a 3D printer (MarketBot) plastic cap to fit the cuvette. Prior to each experiment, the electrodes were cleaned electrochemically in anhydrous ethanol by applying 10 cycles of an alternating potential from −1.0 V to +1.0 V with 100 mV/s. All measurements were run against ferrocene to set the scale. The potential range was scanned from −0.5 to 2.3 V vs ferrocene. Ferrocene cyclic voltammetry scan in iFOS is shown in Fig. S1, Supplementary Information.

2.1.5. Threshold oxidation potential measurements of probes

For the threshold oxidation potential measurements, 2 mL of ethanol, 100 µL of hydrocyanine solution in ethanol, 200 µL of supporting electrolyte sodium hexafluorophosphate ($NaPF_6$) (100 mM in ethanol) were mixed together in a 4 mL plastic cuvette. First, absorption spectra were recorded to determine the concentrations of the dyes in the cuvette using molar absorptivities of the hydrocyanine dyes at 395 nm. Second, the argon was bubbled through the solution for 10–15 s to remove traces of air. Finally, fluorescence intensity recorded at the wavelengths close to the maximum of fluorescence was synchronized with the applied potential.

2.2. Animal experimental design and procedures

All animal surgeries were conducted in compliance with the Washington University Institutional Animal Studies Committee and NIH guidelines. Animals were housed in a central animal care facility and provided with food (PicoLab rodent diet 20, Purina Mills Nutrition International) and water ad libitum. A total of 24 adult male Sprague-Dawley rats (200–250 g, Charles River Laboratories) were randomized to one of three studies for a total of eight groups.

2.2.1. Injection preparation

The reduced dye was synthesized as described above, protected under argon, and kept in −80 °C. It was used for imaging studies within a week after preparation. The resuspension of the dye to form an injectable imaging solution was performed within 4 h of animal injection. For that, the dye was first re-suspended in DMSO to reach 5 mM concentration. The solution was further diluted with ethanol to 2.5 mM and kept as stock solution. The dyes readily dissolved in this medium (50:50 vol. DMSO: ethanol) at this concentration without any visible precipitate. The stock solution was then filtered through syringe filters, pore size 0.45 µm (Millipore) to provide 2.5 mM sterilized stock solution. After that, 80 µL of the filtered stock solution, 400 µL of polyethylene glycol (PEG-400), and 1520 µL of Milli-Q water (resistivity 18.2 MΩ cm) were mixed in a vial to make a final injectable solution at 100 µM dye concentration ready for injection. Imaging was always performed with a freshly prepared solution within less than 4 h after preparation.

2.2.2. Model of acute stress

Rats were restrained and received an intraperitoneal (IP) injection of saline (0.9% NaCl in water) (100 µL). This procedure was used 30 mins or 24 h before the imaging studies to measure ROS within nerve and/or other tissue analysis. This procedure results in a mild amount of acute psychological stress and physical pain (somatic and visceral) to the animals [27]. The control group were handled but received no IP injection before the additional procedures.

2.2.3. Study A: probe delivery

This study considered intraneural probe delivery approach to administer quenched hydrocyanine ROS probe into peripheral nerves. Three groups of rats were utilized in this arm of the study. In Group 1 (diffuse injection; n=2), a needle of microsyringe (Hamilton, 26G) was inserted the length of the nerve under the epineurial sheath and probe injected gradually as the syringe was drawn through the tissue. This technique sought to maximize delivery and distribution of the imaging probe throughout the tissue. In Group 2 (point injection; n=1), the needle was inserted into a single small area under the epineurial sheath and probe injected. This technique intended to minimize physical trauma to the nerve while still administering dye that could diffuse throughout the nerve. In Group 3 (injection control; n=2), a need was inserted the length of the nerve under the epineurial sheath with injection of saline (40 µL) instead of probe.

The presence of ROS within peripheral nerve was detected by macroscopic imaging of anesthetized rats with imaging probes injected into the sciatic nerve. Rats were anesthetized using a cocktail of ketamine (75 mg/kg, Fort Dodge Animal Health) and dexmedetomidine (0.5 mg/kg, Pfizer Animal Health) given subcutaneously. Procedures were conducted with aseptic technique using an operating microscope. The right hindquarter was shaved and prepped with betadine, skin divided parallel to the femur, and the biceps femoris muscle split. Under 10–25× magnification using sterilized microinstruments, the sciatic nerve was exposed to include the sciatic notch proximally and its trifurcation to tibial, peroneal, and sural nerves distally. The probe (1 mM, 40 µL) was injected just under the epineurial sheath of the nerve and imaged (methods below). Following imaging, rats were euthanized with injections of somnasol (150 mg/kg, IP, Delmarva Laboratories).

2.2.4. Study B: in vivo imaging of ROS in nerve in an acute stress model

This study served to demonstrate the ability of the imaging probes to detect ROS within nerve under acute stress utilizing two groups. Group 4 (Stressed; n=4) rats were restrained and received an IP injection of saline (100 µL) 24 h before procedures to measure ROS within nerve. Group 5 (Control; n=4) received no IP injection before these imaging procedures. The presence of elevated ROS within peripheral nerve was detected by macroscopic imaging of anesthetized

rats with imaging probes injected into the sciatic nerve. Rats were anesthetized and imaged 24 h after treatments. Following imaging, rats were euthanized and the sciatic nerve and nerve roots L4 and L5 dorsal root ganglia (DRG) were harvested and flash frozen (−70 °C) for further analysis.

2.2.5. Study C: additional analysis of ROS immediately following acute stress

This study served to detect other changes to nerve due to acute stress utilizing two groups. Group 6 (stressed; n=4) rats were restrained and received an IP injection of saline (100 μL) 30 mins before procedures to measure gene expression changes with DRG (L4 and L5). Group 7 (control; n=4) received no IP injection before these procedures. Group 8 (normal; n=4) served as controls, with no sham procedures performed while nerve and DRG were harvested.

2.2.6. Imaging and image analysis

Immediately after imaging probe injection (within an hour), the nerve and surrounding tissue were imaged using a fluorescence-enabled dissecting macroscope (Olympus MVX10) under brightfield and NIR illumination (Cy7 filtercube, Semrock). Image acquisitions were performed using MetaMorph ver. 7.1.0.0 (Molecular Devices). Images were standardized according to magnification (6.3×), exposure time, and orientation. Image analysis was conducted using ImageJ software (Fig. S2, Supplementary Information).

2.3. Histology

Sciatic nerve was harvested after imaging and underwent histomorphometric analysis as previously described [28]. Briefly, nerve was harvested and stored in 3% glutaraldehyde (Polysciences Inc.). The nerves were post-fixed in 1% osmium tetroxide and serially dehydrated in ethanol and propylene oxide. The nerves were then embedded in epoxy (Polysciences), and sectioned on an ultramicrotome into 1 μm cross sections. Slides were counter-stained with 1% toluidine blue dye. The slides were then analyzed at 1000× on a Leitz Laborlux S microscope. The Leco IA32 Image Analysis System (Leco) was utilized to quantify myelinated axon number, density, and myelin width. All analysis was done by an observer blinded to the experimental groups.

2.4. qRT-PCR of gene expression

DRG were harvested from the L4 and L5 nerve roots to assess gene changes within neurons and their axons composing the sciatic nerve. RNA was extracted using Trizol (Life Technologies), chloroform and RNeasy Mini Kit (Qiagen) according to manufacturer's instructions and pooled for each animal from the L4 and L5 DRG. RNA concentration was determined on a NanoDrop 1000 Spectrophotometer (Thermo Scientific) and purity and integrity were assessed on an Agilent 2100 Bioanalyser RNA 6000 using an Agilent Nano total RNA Kit (Agilent Technologies). Genomic DNA contamination was removed through treatment with gDNA Wipeout Buffer (Qiagen) at 42 °C for 2 mins. RNA was then reverse transcribed into complementary DNA per manufacturer's instructions for the High Capacity RNA to DNA by RT2 First Strand Kit (Qiagen). A panel of genes associated with pain and stress was chosen for analysis. This panel was selected based on known gene changes in DRG following nerve constriction (a pain and stress model) to sciatic nerve using microarray [29], RNA-seq [30] and text mining [31] studies. These genes included: protachykinin-1 (*Tac1*), neuropeptide Y (*Npy*), calcitonin gene-related peptide (*Cgrp*), vascular intestinal peptide (*Vip*), Pituitary adenylate cyclase-activating polypeptide (*Pacap*), Galanin (*Gal*), nerve growth factor (*Ngf*), neurotrophic tyrosine kinase receptor type 1 (*Ntrk1*), interleukin-6 (*Il6*), and POU domain, class 4, transcription factor 1 (*Pou4f1*). These genes were examined following applicable treatments described for each group (groups 4–7) with normalization of expression to a housekeeping gene, β-actin (*Actb*) [32]. PCR arrays were performed on a Step One Plus thermocycler (Applied Biosystems) and the data analyzed on Step One Software ver. 2.2.2 (Applied Biosystems). To estimate the mRNA concentrations, the differences in gene expression levels between two different samples were calculated using the comparative delta cross-over threshold (Ct) method. An absolute value of 2 or greater was selected as the minimum criteria for a significant difference in expression levels between groups.

2.4.1. Statistical analysis

All data were compiled as mean ± standard deviation. Data was tested for normality using the Kolmogorov-Smirnov test. An unpaired, two-tailed Student's *t*-test was used to compare data sets. A significance level of $p < 0.05$ was used in all statistical tests performed.

3. Results and discussion

3.1. Selection of ROS probes

Imaging of ROS levels in tissue requires fluorescent probes with suitable redox potentials (sensitivity) and reactivity. Overly sensitive probes will result in fluorescent activation by endogenous reactive species, while probes with low sensitivity will be non-activated and remain non-fluorescent. Given the same sensitivity, probes with higher reactivity are expected to produce stronger signal. For the probe selections, quantitative measurements of sensitivity and reactivity were performed using a recently described iFOS system [26] modified for NIR measurements. In this method, electrochemical oxidation of the non-fluorescent molecules converts them into fluorescent molecules. This conversion is recorded as a function of the applied electrochemical potential. Quantitative parameters derived using this method are Threshold Oxidation Potential (E_g^t) that reflects the sensitivity of the probe toward oxidation and Reactivity (R): ($R=\Delta F/c$) that describes the kinetic ability of the probes to be oxidized under electrochemical conditions. Graphic description of these parameters is shown in Figs. 2 and 3.

The iFOS graphs of the four prepared NIR activatable probes (see structures in Fig. 1) are presented in Fig. 3. It appears from the results plotted that all compounds showed E_g^t values in the narrow range 1.38–1.46 V vs ferrocene, significantly higher potential than for the previously measured commercial visible ROS probes, such as dihydroxyfluorescein (−0.04 V) and dihydrorhodamine-6 G (+0.45 V). High E_g^t values of the NIR probes made them sensitive only to strong

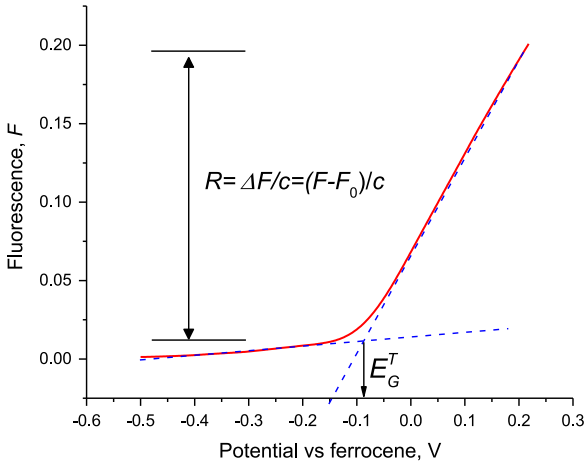

Fig. 2. Principle of measurements of an ROS probe activation using iFOS. Threshold oxidation potential (E_g^t) reflects the sensitivity of the probes toward oxidation. Reactivity (R) reflects the level of the probes activation $R=(F-F_o)/c$ where F is the fluorescence at the maximum measured oxidation potential, F_o – starting fluorescence, c – concentration of the probe. Example is given for dihydroxyfluorescein.

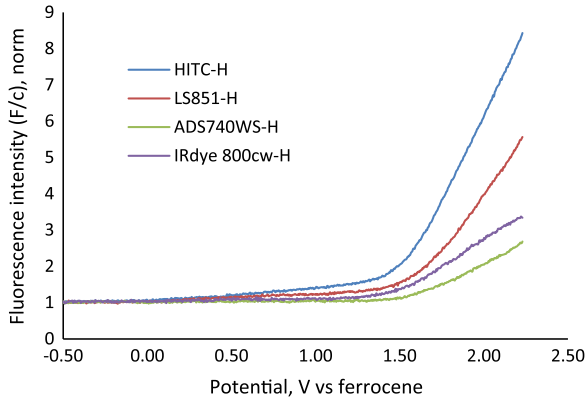

Fig. 3. iFOS of the tested activatable probes. The signal was normalized to the same concentration (1 μM of the probe) and initial fluorescence at −0.5 V. Calculated E_g^t and R values: $E_{g(\text{HITC-H})}^t$=+1.41 V, $R_{\text{HITC-H}}$=8.3; $E_{g(\text{LS851-H})}^t$=+1.40 V, $R_{\text{LS851-H}}$=5.5; $E_{g(\text{ADS740WS-H})}^t$=+1.46 V, $R_{\text{ADS740WS-H}}$=3.3; $E_{g(\text{IRdye800CW-H})}^t$=+1.38 V, $R_{\text{IRdye800CW-H}}$=2.6. Excitation 725 nm, electrochemical ramp 4.5×10^{-3} V/s, total recording time 610 s, solvent ethanol supporting electrolyte $NaPF_6$ (100 mM in ethanol).

radicals, such as hydroxyls (redox potential of the common ROS is given in Table S1, Supplementary Information). Commercially available IRDye800CW-H was the most sensitive among the studied probes with the E_g^t =+1.38 V. However, HITC-H was the most reactive providing twice more signal than IRdye800CW-H or other dyes. In the selection of the probe, we also envisioned that due to its hydrophobic properties, HITC-H and the product of its activation HITC, will not leak from the nerve after interfascicular injection. Hence, for all in vivo studies, HITC-H was selected.

3.2. Optimization of the delivery

We have previously demonstrated intrafascicular injection of cyanine dyes, which did not cause toxicity to the animal or chemical damage to the nerves [33]. To determine a delivery technique of the probe to nerve, we considered two microinjection techniques: diffuse vs point injection. A diffuse technique could maximize distribution of the probe but potentially causes additional tissue damage, while a point injection could minimize tissue damage but may under-distribute the probe within the tissue. Following administration of the probe within nerve using these techniques, the probe signal intensity and location was measured by fluorescence imaging within an hour. In general, the signal generated by the probe from the nerve was > 4× background levels (measured by the average intensity at the region of interest (ROI), see Supplementary Information Fig. S2) reflecting a combination of nerve's autofluorescence, dye's residual fluorescence, and activation of the probe by endogenous oxidation activity in the nerve tissue (Fig. 4). As expected, the diffuse injection resulted in unintended activation of probe throughout the entire region of nerve where the microsyringe passed (Fig. 4, upper panel). Conversely, the point injection resulted in the local accumulation of the probe while still permitting the probe to flow longitudinally within the nerve ~0.5–1.0 cm (Fig. 4, middle panel). Significantly higher level of emission along the entire nerve (nerve to surrounding tissue ratio 6.21 vs 1.34), suggested an activation of the probe by ROS upon delivery. The autofluorescence of the nerve evaluated by the injection of saline into the nerve and comparing to the surrounding tissue was marginal (Ratio nerve/surrounding tissue=1.29; Fig. 4, lowest panel). Therefore, moving forward, we measured ROS within nerves using the point injection

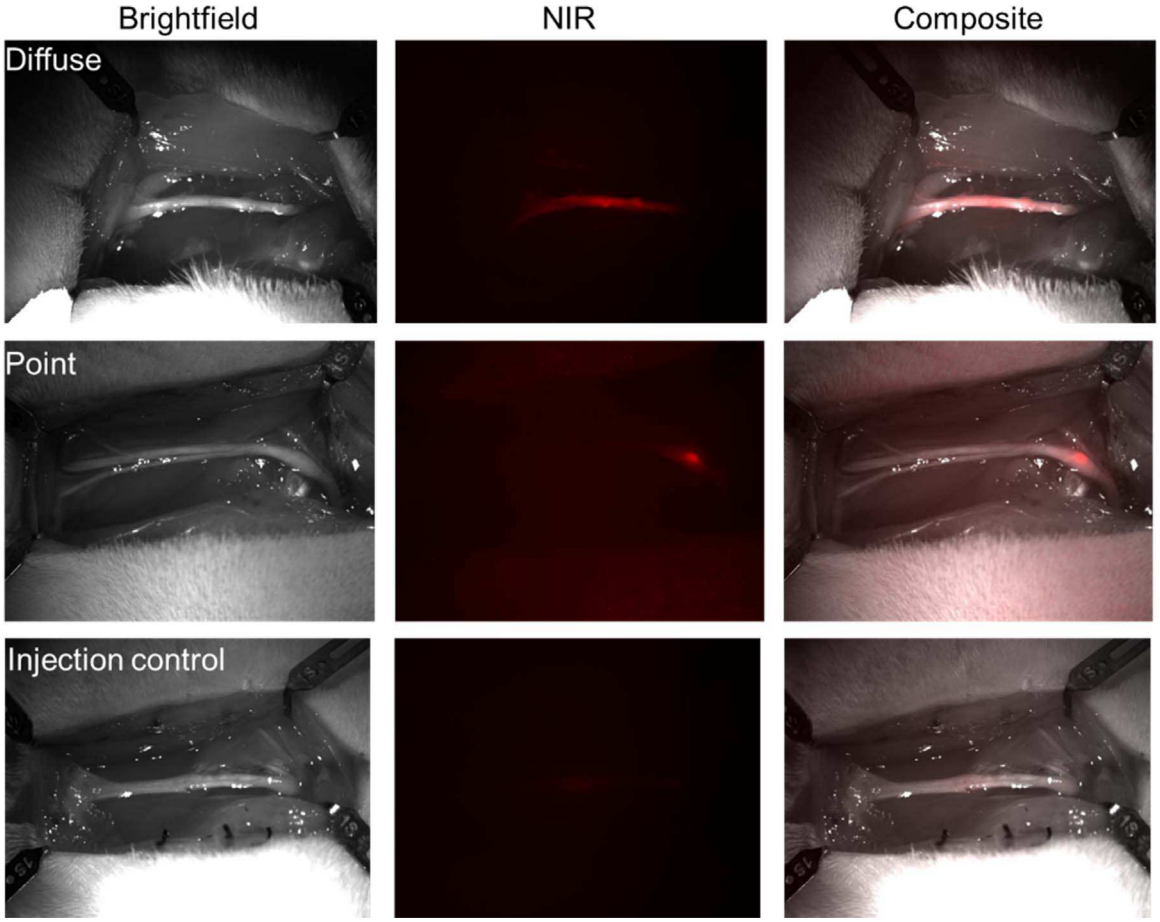

Fig. 4. Activation of HITC-H after interfascicular delivery into sciatic nerve. Upper panel diffuse injection, (nerve to surrounding tissue ratio=6.21). Middle panel, point injection, (ratio=1.34). Lowest panel, diffuse saline injection (ratio=1.29). Images were taken within 1 h from the probe delivery.

technique as it minimized unintended probe activation from normal response to physical damage.

3.3. Imaging of acute stress

Having established the appropriate technique to introduce the probe to nerve, we examined an animal model of acute stress. The effect of acute stress on the PNS is complex and associated with gene expression changes [27] and activation of cytokines, prostanoids and other mediators of inflammation [34]. Within the PNS, upregulated ROS acutely sensitize nociceptors [35], which can activate the "fight and flight" response but can occasionally lead to painful inflammatory conditions. Systematic studies of acute stress, such as caused by physiological stimuli or induced somatic and visceral pain, have identified certain mediators which modify ROS generation including corticotropin-releasing hormone (CRH) [36]. In the CNS, this hormone activates autonomic and endocrine functions that down-regulate immune responses [34]. Peripheral sensory afferent type C fibers and postganglionic sympathetic nerves also express CRH [37]. In contrast to the brain, peripheral CRH exerts pro-inflammatory effects [34]. Specifically, it enhances the expression of nitric oxide synthase to promote nitric oxide production [38] and ROS that induce mast cell degranulation [39].

To generate an acute, psychologically-stressful event, rats were given an IP injection of saline. Twenty four hours following this acute stress event, rat nerve demonstrated robust probe signal compared to unstressed rat nerve (Fig. 5). Significantly larger nerve to background ratios from the stressed animals were observed: ratio=6.21 (Fig. 5, upper panel) vs non-stressed (ratio=1.31) (Fig. 5, lower panel), indicating a substantial increase of ROS in the nerve tissue following acute stress.

3.4. Histological analysis shows minimal changes to nerve after acute stress

To determine how the sciatic nerve was affected by the stressful event, more common biological outcome metrics were considered. Quantitative histology of the nerve 24 h after acute stress was measured immediately following imaging. While the injection of probe and fluid had an impact on the myelinated fiber spacing, major morphological features to nerve remained unchanged (Fig. 6, upper panel).

The morphology of the nerve after the acute stress had statistically identical parameters to Control group nerves, indicating that the stress did not induce any alterations to nerve morphology with no evidence of injury (Fig. 6, lowest panel). The differences in the total number of myelinated axons, myelinated axon density, and myelin width were overall unremarkable. A small variability in the morphometric parameters is expected, as a result of natural biological variability between animals.

3.5. Gene expression analysis detects minimal changes to nerve after acute stress

In addition, gene expression changes were measured in sensory neurons (DRG), which project axons in the sciatic nerve. These gene changes were measured shortly after the stressful event (30 min) as well as at the time (24 h) corresponding with the observed ROS signal following the stressful event. A panel of genes associated with pain and stress (Table 1) was chosen for analysis according to the literature reports of most common alterations associated with neural damage [29–31]. While most genes in the DRG were unchanged in expression following the stressful event, nerve growth factor (NGF) gene expression was decreased immediately following the stress (30 mins) before returning to normal expression levels. This observation is congruent with other reports, where circulating and brain NGF levels undergo significant variations after exposure to stressful events [40] (also reviewed [41]). Therefore, the described ROS imaging approach with activatable fluorescent probes offers an opportunity to observe minimal discrete changes to tissue that could go overlooked using more common outcome metrics.

4. Conclusions and future work

Acute stress in rats caused by intraperitoneal injection of saline caused a significant increase in intraneural ROS as measured and visualized in sciatic nerves of living rat 24 h after the stress. The effect was visualized in vivo using a novel approach consisting of NIR fluorescence molecular probes directly injected into peripheral nerves. The probes demonstrated rapid activation in nerve after injection and

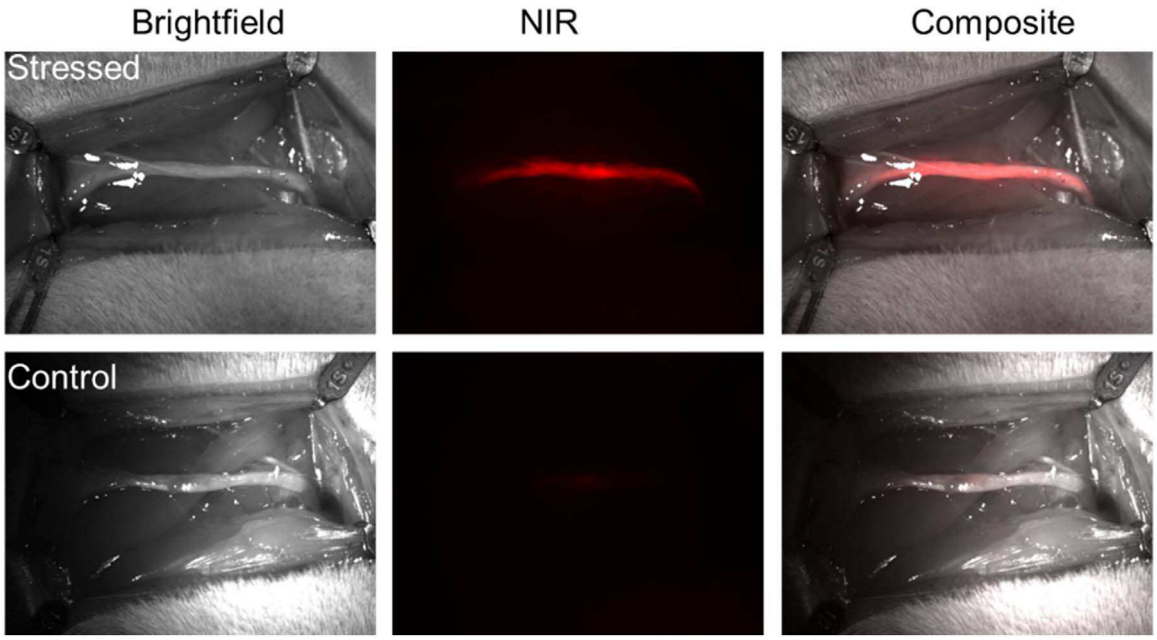

Fig. 5. Effect of acute stress on HITC-H activation in sciatic nerves. Upper panel: stress induced by an injection of saline ip leads to strong activation of the probe (ratio=6.21), Lower panel: no activation is observed in control (non-stressed) mice (ratio=1.31). Images were collected 24 h after the stress.

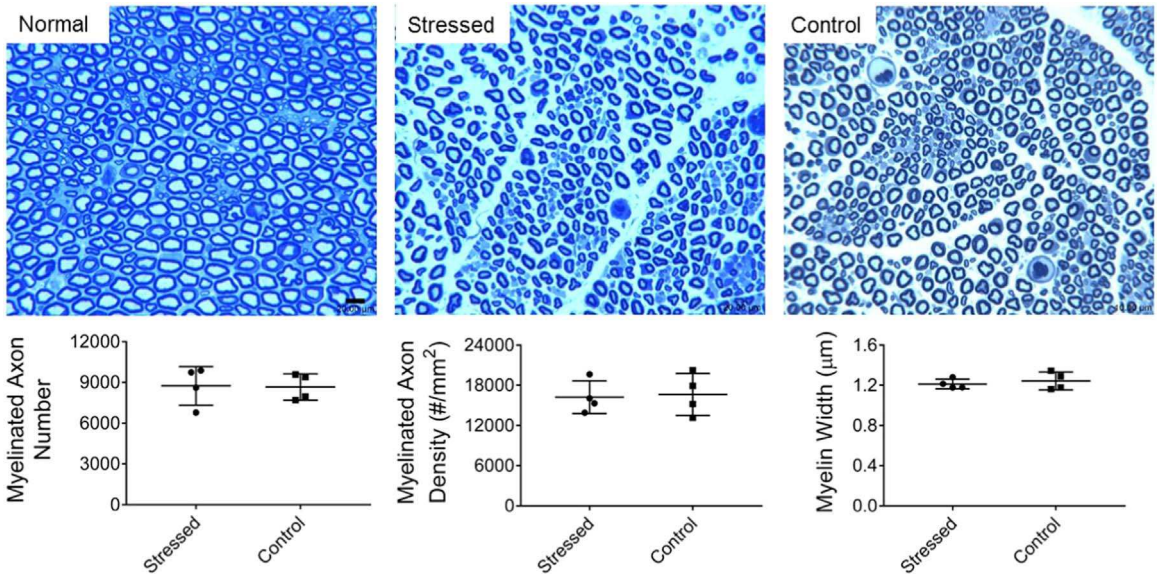

Fig. 6. Morphology of sciatic nerves after acute stress. Upper row: histological micrographs. *Normal*: sciatic nerve of non-stressed mice with no injection of the probe. *Stressed*: stressed sciatic nerve 24 h following stress, harvested immediately after imaging. *Control*: sciatic nerve harvested immediately after imaging the probe injected into nerve, no stress. Stained with osmium tetroxide, counterstained with toluidine blue. Obj. 40×, overall magnification 400×. Lower row: corresponding histomorphometric analysis of sciatic nerve cross-sections after acute stress, where no differences were noted compared to control and normal.

Table 1
Relative DRG gene expression changes following acute stress (fold change vs normal DRG).

	Experimental groups (mean ± SD)			Statistics (n=4 per group, p value)	
Gene of interest	**Control**	**Stress 30 min**	**Stress 24 h**	**Stress vs control, 30 min**	**Stress vs control, 24 h**
Neuropeptides					
Tac1	1 ± 0.07	1.07 ± 0.1	1.17 ± 0.2	NS	NS
Npy	1 ± 0.4	0.7 ± 0.4	0.82 ± 0.88	NS	NS
Cgrp	1 ± 0.08	1.04 ± 0.07	1.01 ± 0.2	NS	NS
Vip	1 ± 0.6	1.04 ± 0.2	1.08 ± 0.2	NS	NS
Pacap	1 ± 0.1	1.1 ± 0.09	1.3 ± 0.13	NS	NS
Galanin	1 ± 0.1	0.95 ± 0.26	1.08 ± 0.17	NS	NS
Neurotrophic factors and receptors					
Ngf	1 ± 0.13	**(−2.44) ± 1.29**	1 ± 0.2	**0.039**	NS
Ntrk1	1 ± 0.1	1.05 ± 0.1	1.02 ± 0.14	NS	NS
Proinflammatory cytokine					
Il6	1 ± 0.2	0.87 ± 0.1	1 ± 0.3	NS	NS
Transcription factor involved in cell damage and apoptosis					
Pou4f1	1 ± 0.16	1 ± 0.07	0.9 ± 0.04	NS	NS

reported significantly higher activation after acute stress. Other techniques such as histomorphometry and gene expression analysis for pain and stress associated genes had minimal ability to detect changes to nerve shortly after acute stress, with exception of *Ngf* expression in DRG, which was decreased shortly after acute stress before returning to basal levels. Overall, the results suggest an imaging approach with activatable fluorescent probes can be used for evaluation and monitoring acute stress in animal models. The described technique will facilitate discovery of new neuroprotective interventions to reduce the damaging effects of physical, psychological and pharmacological stress on the nervous system. Improvements over the intrafascicular injection route described here such as non-invasive topical delivery [42] and minimally invasive injectable nerve-targeted [43] fluorescent reporters are currently under investigation as more clinically viable options.

Conflict of interest

No benefit of any kind will be received either directly or indirectly by the author(s). The authors declare no competing financial interests.

Acknowledgment

We thank National Cancer Insitute/National Institutes of Health: CA198419 (MB) and U54CA199092; Foundation for Barnes-Jewish Hospital Cancer Frontier Fund; National Science Foundation Research Infrastructure Improvement Award #IIA-1355406 for the financial support and the Washington University Optical Spectroscopy Core Facility (NIH 1S10RR031621-01) for assisting with the optical measurements.

Appendix A. Supplementary material

Supplementary data associated with this article can be found in the online version at http://dx.doi.org/10.1016/j.freeradbiomed.2016.09.028.

References

[1] K.A. Whyte, R.C. Hogg, J. Dyavanapalli, A.A. Harper, D.J. Adams, Reactive oxygen species modulate neuronal excitability in rat intrinsic cardiac ganglia, Auton. Neurosci. 150 (1–2) (2009) 45–52.
[2] Z. Radak, K. Suzuki, M. Higuchi, L. Balogh, I. Boldogh, E. Koltai, Physical exercise,

reactive oxygen species and neuroprotection, Free Radic. Biol. Med.
[3] N. Suzuki, R. Mittler, Reactive oxygen species-dependent wound responses in animals and plants, Free Radic. Biol. Med. 53 (12) (2012) 2269–2276.
[4] A.H. Jacobs, B. Tavitian, I.N. Consortium, Noninvasive molecular imaging of neuroinflammation, J. Cereb. Blood Flow Metab. 32 (7) (2012) 1393–1415.
[5] S. Adachi, K. Kawamura, K. Takemoto, Oxidative damage of nuclear DNA in liver of rats exposed to psychological stress, Cancer Res. 53 (18) (1993) 4153–4155.
[6] A. Barascu, C. Le Chalony, G. Pennarun, D. Genet, N. Imam, B. Lopez, P. Bertrand, Oxidative stress induces an ATM-independent senescence pathway through p38 MAPK-mediated lamin B1 accumulation, Embo J. 31 (5) (2012) 1080–1094.
[7] T. Kalogeris, C.P. Baines, M. Krenz, R.J. Korthuis, Cell biology of ischemia/reperfusion injury, Int. Rev. Cell. Mol. Biol. 298 (2012) 229–317.
[8] B. Parajuli, Y. Sonobe, H. Horiuchi, H. Takeuchi, T. Mizuno, A. Suzumura, Oligomeric amyloid beta induces IL-1beta processing via production of ROS: implication in Alzheimer's disease, Cell Death Dis. 4 (2013) e975.
[9] M.A. Friese, B. Schattling, L. Fugger, Mechanisms of neurodegeneration and axonal dysfunction in multiple sclerosis, Nat. Rev. Neurol. 10 (4) (2014) 225–238.
[10] E. Pollari, G. Goldsteins, G. Bart, J. Koistinaho, R. Giniatullin, The role of oxidative stress in degeneration of the neuromuscular junction in amyotrophic lateral sclerosis, Front. Cell. Neurosci. 8 (2014) 131.
[11] C.B. Wilson, L.D. McLaughlin, P.J. Ebenezer, A.R. Nair, J. Francis, Valproic acid effects in the hippocampus and prefrontal cortex in an animal model of post-traumatic stress disorder, Behav. Brain Res. 268 (2014) 72–80.
[12] L. Di, Cesare Mannelli, M. Zanardelli, P. Failli, C. Ghelardini, Oxaliplatin-induced neuropathy: oxidative stress as pathological mechanism. Protective effect of silibinin, J. Pain 13 (3) (2012) 20276–20284.
[13] E.L. Feldman, Oxidative stress and diabetic neuropathy: a new understanding of an old problem, J. Clin. Investig. 111 (4) (2003) 431–433.
[14] T. Kanda, Biology of the blood-nerve barrier and its alteration in immune mediated neuropathies, J. Neurol. Neurosurg. Psychiatry 84 (2) (2013) 208–212.
[15] J.A. Kiernan, Vascular permeability in the peripheral autonomic and somatic nervous systems: controversial aspects and comparisons with the blood-brain barrier, Microsc. Res. Tech. 35 (2) (1996) 122–136.
[16] H.J. Jun, S. Woolfenden, S. Coven, K. Lane, R. Bronson, D. Housman, A. Charest, Epigenetic regulation of c-ROS receptor tyrosine kinase expression in malignant gliomas, Cancer Res. 69 (6) (2009) 2180–2184.
[17] L.L. Thomsen, D.W. Miles, L. Happerfield, L.G. Bobrow, R.G. Knowles, S. Moncada, Nitric oxide synthase activity in human breast cancer, Br. J. Cancer 72 (1) (1995) 41–44.
[18] K. Thusu, E. Abdel-Rahman, P. Dandona, Measurement of reactive oxygen species in whole blood and mononuclear cells using chemiluminescence, in: D. Armstrong (Ed.)Free Radical and Antioxidant Protocols, Humana Press, Totowa, NJ, 1998, pp. 57–62.
[19] S. Dikalov, K.K. Griendling, D.G. Harrison, Measurement of reactive oxygen species in cardiovascular studies, Hypertension 49 (4) (2007) 717–727.
[20] K. Kundu, S.F. Knight, N. Willett, S. Lee, W.R. Taylor, N. Murthy, Hydrocyanines: a. Class of fluorescent sensors that can image reactive oxygen species in cell culture, tissue, and in vivo, Angew. Chem. Int. Ed. Engl. 48 (2) (2009) 299–303.
[21] S. Magalotti, T.P. Gustafson, Q. Cao, D.R. Abendschein, R.A. Pierce, M.Y. Berezin, W.J. Akers, Evaluation of inflammatory response to acute ischemia using near-infrared fluorescent reactive oxygen sensors, Mol. Imaging Biol. 15 (4) (2013) 423–430.
[22] H. Zhou, S. He, S. Gunsten, S. Brody, W. Akers, M. Berezin, NIR fluorescent contrast agents for detection of inflammation of lungs in vivo, CLEO: applications and technology, Opt. Soc. Am. 1 (2014) AM2P.
[23] P.W. Lin, L.E.S. Myers, L. Ray, S.-C. Song, T.R. Nasr, A.J. Berardinelli, K. Kundu, N. Murthy, J.M. Hansen, A.S. Neish, Lactobacillus rhamnosus blocks inflammatory signaling in vivo via reactive oxygen species generation, Free Radic. Biol. Med. 47 (8) (2009) 1205–1211.
[24] S. Suri, S.M. Lehman, S. Selvam, K. Reddie, S. Maity, N. Murthy, A.J. García, In vivo fluorescence imaging of biomaterial-associated inflammation and infection in a minimally invasive manner, J. Biomed. Mater. Res. A 103 (1) (2015) 176–183.
[25] T.P. Gustafson, Q. Cao, S. Achilefu, M.Y. Berezin, Defining a polymethine dye for fluorescence anisotropy applications in the near-infrared spectral range, Chemphyschem 13 (3) (2012) 716–723.
[26] S.T. Wang, N.G. Zhegalova, T.P. Gustafson, A. Zhou, J. Sher, S. Achilefu, O.Y. Berezin, M.Y. Berezin, Sensitivity of activatable reactive oxygen species probes by fluorescence spectroelectrochemistry, Analyst 138 (15) (2013) 4363–4369.
[27] A.E. Ryabinin, Y.M. Wang, D.A. Finn, Different levels of Fos immunoreactivity after repeated handling and injection stress in two inbred strains of mice, Pharmacol. Biochem. Behav. 63 (1) (1999) 143–151.
[28] D.A. Hunter, A. Moradzadeh, E.L. Whitlock, M.J. Brenner, T.M. Myckatyn, C.H. Wei, T.H. Tung, S.E. Mackinnon, Binary imaging analysis for comprehensive quantitative histomorphometry of peripheral nerve, J. Neurosci. Methods 166 (1) (2007) 116–124.
[29] H.-S. Xiao, Q.-H. Huang, F.-X. Zhang, L. Bao, Y.-J. Lu, C. Guo, L. Yang, W.-J. Huang, G. Fu, S.-H. Xu, X.-P. Cheng, Q. Yan, Z.-D. Zhu, X. Zhang, Z. Chen, Z.-G. Han, X. Zhang, Identification of gene expression profile of dorsal root ganglion in the rat peripheral axotomy model of neuropathic pain, Proc. Natl. Acad. Sci. USA 99 (12) (2002) 8360–8365.
[30] J.R. Perkins, A. Antunes-Martins, M. Calvo, J. Grist, W. Rust, R. Schmid, T. Hildebrandt, M. Kohl, C. Orengo, S.B. McMahon, D.L.H. Bennett, A comparison of RNA-seq and exon arrays for whole genome transcription profiling of the L5 spinal nerve transection model of neuropathic pain in the rat, Mol. Pain. 10 (2014) (7-7).
[31] D.G. Jamieson, A. Moss, M. Kennedy, S. Jones, G. Nenadic, D.L. Robertson, B. Sidders, The pain interactome: connecting pain-specific protein interactions, PAIN 155 (11) (2014) 2243–2252.
[32] O. Thellin, W. Zorzi, B. Lakaye, B. De Borman, B. Coumans, G. Hennen, T. Grisar, A. Igout, E. Heinen, Housekeeping genes as internal standards: use and limits, J. Biotechnol. 75 (2–3) (1999) 291–295.
[33] T.P. Gustafson, Y. Yan, P. Newton, D.A. Hunter, S. Achilefu, W.J. Akers, S.E. Mackinnon, P.J. Johnson, M.Y. Berezin, A NIR dye for development of peripheral nerve targeted probes, Med. Chem. Commun. 3 (6) (2012) 685–690.
[34] G.P. Chrousos, The hypothalamic–pituitary–adrenal axis and immune-mediated inflammation, N. Engl. J. Med. 332 (20) (1995) 1351–1363.
[35] B.L. Kidd, L.A. Urban, Mechanisms of inflammatory pain, Br. J. Anaesth. 87 (1) (2001) 3–11.
[36] R.B.S. Harris, Chronic and acute effects of stress on energy balance: are there appropriate animal models?, Am. J. Physiol. 308 (4) (2015) R250–R265.
[37] R. Udelsman, J.P. Harwood, M.A. Millan, G.P. Chrousos, D.S. Goldstein, R. Zimlichman, K.J. Catt, G. Aguilera, Functional corticotropin releasing factor receptors in the primate peripheral sympathetic nervous system, Nature 319 (6049) (1986) 147–150.
[38] M. Nezi, G. Mastorakos, Z. Mouslech, L.J. De Groot, P. Beck-Peccoz, G. Chrousos, K. Dungan, A. Grossman, J.M. Hershman, C. Koch, R. McLachlan, M. New, R. Rebar, F. Singer, A. Vinik, M.O. Weickert (Eds.), Corticotropin releasing hormone and the immune/inflammatory response, Endotext, South Dartmouth, MA, 2000.
[39] J. Cao, N. Papadopoulou, D. Kempuraj, W.S. Boucher, K. Sugimoto, C.L. Cetrulo, T.C. Theoharides, Human mast cells express corticotropin-releasing hormone (CRH) receptors and CRH leads to selective secretion of vascular endothelial growth factor, J. Immunol. 174 (12) (2005) 7665–7675.
[40] S. von Richthofen, U.E. Lang, R. Hellweg, Effects of different kinds of acute stress on nerve growth factor content in rat brain, Brain Res. 987 (2) (2003) 207–213.
[41] L. Aloe, E. Alleva, M. Fiore, Stress and nerve growth factor: findings in animal models and humans, Pharmacol. Biochem. Behav. 73 (1) (2002) 159–166.
[42] L.L. Jorge, C.C. Feres, V.E. Teles, Topical preparations for pain relief: efficacy and patient adherence, J. Pain Res. 4 (2011) 11–24.
[43] M.H. Park, H. Hyun, Y. Ashitate, H. Wada, G. Park, J.H. Lee, C. Njiojob, M. Henary, J.V. Frangioni, H.S. Choi, Prototype nerve-specific near-infrared fluorophores, Theranostics 4 (8) (2014) 823–833.